REPORT

MEMORY RESEARCH

Engrams and circuits crucial for systems consolidation of a memory

Takashi Kitamura,[1]* Sachie K. Ogawa,[1]* Dheeraj S. Roy,[1]* Teruhiro Okuyama,[1] Mark D. Morrissey,[1] Lillian M. Smith,[1] Roger L. Redondo,[1,2]† Susumu Tonegawa[1,2]‡

Episodic memories initially require rapid synaptic plasticity within the hippocampus for their formation and are gradually consolidated in neocortical networks for permanent storage. However, the engrams and circuits that support neocortical memory consolidation have thus far been unknown. We found that neocortical prefrontal memory engram cells, which are critical for remote contextual fear memory, were rapidly generated during initial learning through inputs from both the hippocampal–entorhinal cortex network and the basolateral amygdala. After their generation, the prefrontal engram cells, with support from hippocampal memory engram cells, became functionally mature with time. Whereas hippocampal engram cells gradually became silent with time, engram cells in the basolateral amygdala, which were necessary for fear memory, were maintained. Our data provide new insights into the functional reorganization of engrams and circuits underlying systems consolidation of memory.

Memories are thought to be initially stored within the hippocampal–entorhinal cortex (HPC-EC) network (recent memory) and, over time, slowly consolidated within the neocortex for permanent storage (remote memory) (*1*–*7*). Systems memory consolidation models suggest that the interaction between the HPC-EC network and the neocortex during and after an experience is crucial (*8*–*12*). Experimentally, prolonged inhibition of hippocampal or neocortical networks during the consolidation period produces deficits in remote memory formation (*13*–*15*). However, little is known regarding specific neural circuit mechanisms underlying the formation and maturation of neocortical memories through interactions with the HPC-EC network. Using activity-dependent cell-labeling technology (*16*–*18*), combined with viral vector–based transgenic, anatomical (*19*, *20*), and optogenetic strategies (*19*, *21*) for circuit-specific manipulations and in vivo calcium imaging (*22*), we investigated the nature and dynamics of neocortical and subcortical memory engram cells [a population of neurons that are activated by learning, have enduring cellular changes, and are reactivated by a part of the original stimuli for recall (*18*)] and their circuits for systems consolidation of memory.

We first traced entorhinal projections to frontal cortical structures [the medial prefrontal cortex (PFC), caudal anterior cingulate cortex (cACC), and retrosplenial cortex (RSC)] involved in contextual fear memory, as well as to the basolateral amygdala (BLA), with injections of the retrograde tracer cholera toxin subunit B–Alexa*555* (hereafter, CTB injections) into these regions (fig. S1). CTB injections resulted in labeling in the medial entorhinal cortex (MEC), specifically in cells in layer Va (Fig. 1, A to D and H, and fig. S2, A to D), indicating that MEC-Va cells have extensive projections to the neocortex and BLA (*23*). We then sought to inhibit these specific projections by bilaterally injecting adeno-associated virus 8 (AAV_8)–calcium/calmodulin-dependent protein kinase II (CaMKII):eArchT–enhanced yellow fluorescent protein (eYFP) in the deep layers of the MEC in wild-type (WT) mice with bilaterally implanted optic fibers above the PFC, cACC, or RSC (Fig. 1, E and J, and fig. S2G). Expression of eArchT-eYFP was abundant in MEC-Va terminals located in each of these regions (Fig. 1, B and I, and fig. S2D). These mice were then subjected to contextual fear conditioning (CFC) while we delivered green light bilaterally to the different cortical areas that have MEC-Va projections during either the conditioning period (day 1) (fig. S2E) or the recall test period (days 2, 8, 15, and 22) (fig. S2F). Axon terminal inhibition with optogenetics of MEC-Va cells within the PFC during day 1 of CFC disrupted memory at days 15 and 22, but not at days 2 or 8 (Fig. 1F). Terminal inhibition during memory recall tests did not affect memory retrieval (Fig. 1G). Last, terminal inhibition in the cACC or RSC during CFC or recall had no effect on memory throughout these periods (Fig. 1, J to L, and fig. S2, G to I).

The above results suggest that MEC-Va input into the PFC during CFC is crucial for the eventual formation of remote memory. This hypothesis was supported by several findings. First, CFC increased the number of c-Fos^+ cells in the PFC compared with that in the PFC of home-cage mice (Fig. 1, M to O), whereas context-only exposure did not increase c-Fos activity in the PFC (Fig. 1O). Second, optogenetic terminal inhibition of MEC-Va projections within the PFC during CFC inhibited the observed increase of c-Fos^+ cells in the PFC (Fig. 1O). Last, we identified CFC engram cells in the PFC. We targeted injections of AAV_9–c-fos:tetracycline-controlled transactivator (tTA) and AAV_9–tetracycline response element (TRE):channelrhodopsin-2 (ChR2)–mCherry (Fig. 1, P and Q) and optic fibers to the PFC of WT mice and labeled the PFC cells activated by CFC with ChR2 while the mice were off doxycycline (Fig. 1R). Blue light stimulation at 4 Hz, but not at the conventional 20 Hz, of ChR2-mCherry–expressing cells in the PFC induced increased freezing behavior on days 2 and 12 in an unconditioned context (Fig. 1S and fig. S3), compared with freezing under the blue light–off condition. This blue light–induced freezing was prevented when MEC-Va fibers in the PFC were inhibited during CFC on day 1 (Fig. 1, T and U, and fig. S4). Using transsynaptic retrograde tracing combined with the activity-dependent cell labeling, we confirmed that the PFC engram cells generated by CFC received monosynaptic input from MEC-Va cells (Fig. 1, V to X, and fig. S5).

To examine whether PFC engram cells are also reactivated by the conditioned context (rather than by blue light) at recent and remote time points, we targeted injections of AAV_9-TRE:human histone H2B–green fluorescent protein (H2B-GFP) to the PFC of c-fos:tTA transgenic mice (Fig. 2A). The mice underwent CFC on day 1 and then were reexposed to the conditioned (context A) or an unconditioned (context B) context on days 2 or 13 (Fig. 2B). Cells activated by CFC were labeled with H2B-GFP, and the cells activated by the context test were labeled with a c-Fos antibody; we calculated the proportion of double-labeled cells (Fig. 2, A to B, and fig. S6B). Compared with H2B-GFP^- cells, H2B-GFP^+ cells (PFC engram cells) were preferentially reactivated in context A on day 13, but not on day 2 (Fig. 2C). There was no difference in c-Fos expression between H2B-GFP^+ and H2B-GFP^- cells when mice were tested in context B (Fig. 2C). We also found that the spine density of the PFC engram cells on day 12 was significantly higher than on day 2 (Fig. 2, D and E, and fig. S7), in line with previous findings of a positive correlation between the dendritic spine density of memory engram cells and memory expression triggered by natural recall cues (*24*–*26*).

To test whether PFC engram cells are necessary for memory recall by natural cues, we bilaterally targeted injections of AAV_9–c-fos:tTA and AAV_9-TRE:ArchT-eGFP (Fig. 2, D and F) and optic fibers to the PFC of WT mice and labeled the PFC engram cells that were activated by CFC with ArchT while the mice were off doxycycline (Fig. 2F). Cell body inhibition of the

[1]RIKEN-MIT Center for Neural Circuit Genetics at the Picower Institute for Learning and Memory, Departments of Biology and Brain and Cognitive Sciences, Massachusetts Institute of Technology, Cambridge, MA 02139, USA. [2]Howard Hughes Medical Institute, Massachusetts Institute of Technology, Cambridge, MA 02139, USA.
*These authors contributed equally to this work. †Present address: Roche Pharmaceutical Research and Early Development, Roche Innovation Center, F. Hoffmann-La Roche, Basel, Switzerland.
‡Corresponding author. Email: tonegawa@mit.edu

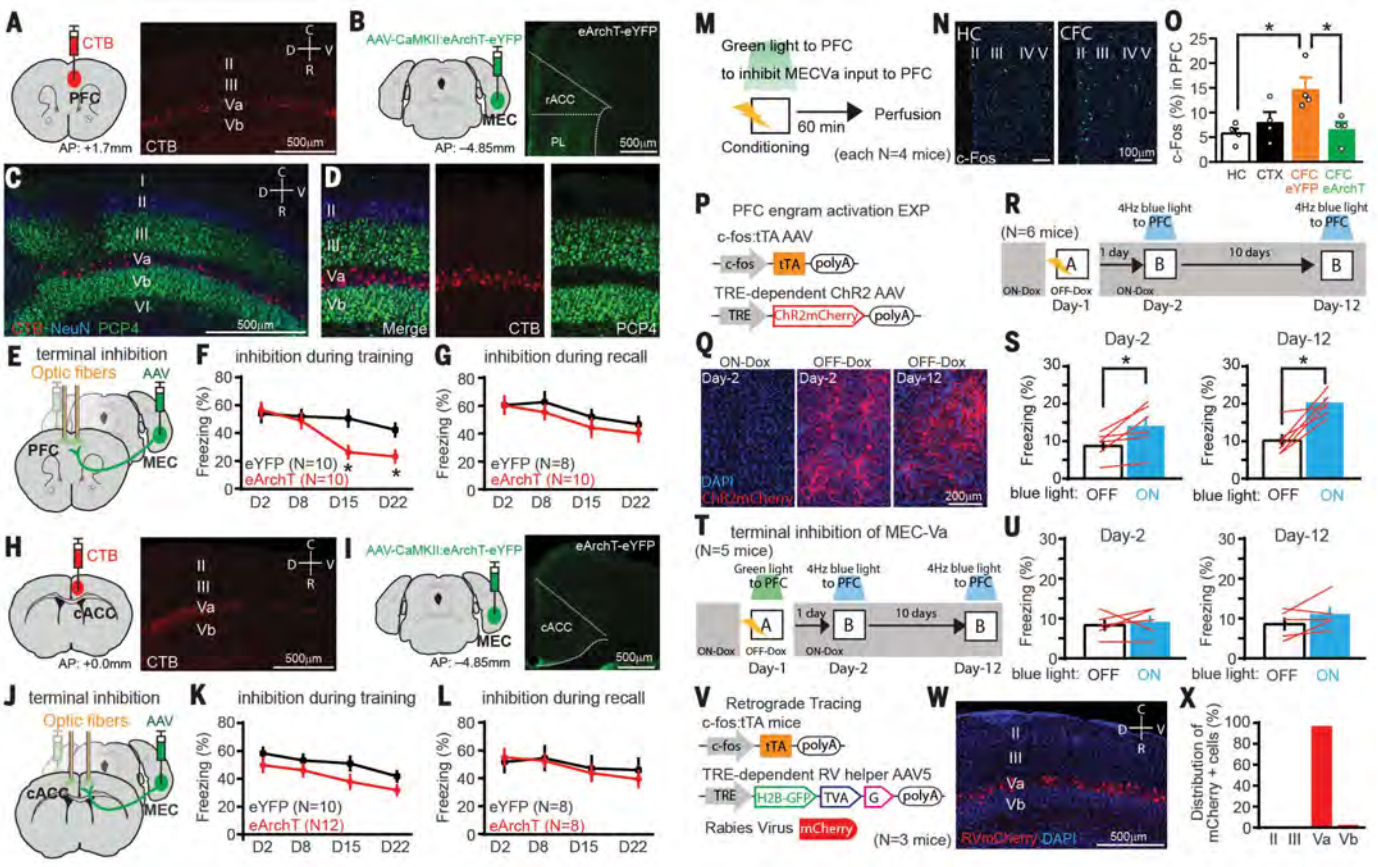

Fig. 1. MEC-Va input to the PFC during conditioning is crucial for generation of PFC engram cells. (**A**) CTB injection into the PFC (left) and sagittal section of the MEC with CTB-labeled cells (red) (right). AP, anterior posterior; C, caudal; R, rostral; D, dorsal; V, ventral. (**B**) AAV_8-CaMKII:eArchT-eYFP injection into the MEC (left) and coronal sections of PFC with MEC-Va axons expressing eYFP (green) (right). rACC, rostral ACC; PL, prelimbic cortex. (**C** and **D**) Sagittal section of MEC with CTB-labeled cells (red), immunostained with anti-PCP4 (green) and anti-NeuN (blue). PCP4 is a marker for layer III and Vb cells in MEC. The images were produced following CTB injection into the BLA. (**E** and **J**) Viral injections and optic fiber implantations. (**F** and **G**) Time courses (D, day) of freezing during recall tests. Green light was shone into the PFC during conditioning (F) or testing (G). (**H**) CTB injection into caudal ACC (cACC) (left) and sagittal section of the MEC with CTB-labeled cells (red) (right). (**I**) AAV_8-CaMKII:eArchT-eYFP injection into the MEC (left) and coronal sections of cACC with MEC-Va axons (green) (right). (**K** and **L**) Time courses of freezing during recall tests. Green light was shone into the cACC during conditioning (K) or testing (L). (**M**) Experimental schedule. (**N**) Coronal section of PFC with anti–c-Fos (green). HC, home cage; CFC, contextual fear conditioning. (**O**) Percentages of c-Fos^+ cells in the PFC of the HC, context exposure (CTX), CFC with eYFP, and CFC with eArchT groups. (**P**) Virus-mediated engram cell labeling with ChR2. (**Q**) Coronal section of PFC with ChR2-mCherry (red). (**R** and **T**) Experimental schedules. (**S** and **U**) Averaged freezing for blue light–off and blue light–on epochs. (**V**) Retrograde transsynaptic labeling with activity-dependent cell labeling. (**W**) Sagittal section of MEC with rabies virus–specific mCherry (red). (**X**) Distribution of 212 $mCherry^+$ cells in the MEC. $^*P < 0.05$; unpaired *t* test compared with eYFP [(F), (G), (K), and (L)], one-way analysis of variance (ANOVA) with Tukey-Kramer test (O), or paired *t* test [(S) and (U)]. Graphs show means ± SEM (in the bar graphs, circles and red lines represent individual animals). Lightning bolt, footshock; polyA, polyadenylation signal; DAPI, 4′,6-diamidino-2-phenylindole; "A", context A (conditioned context); "B", context B (unconditioned context); OFF-Dox, off doxycycline; ON-Dox, on doxycycline.

PFC engram cells by green light during retrieval did not affect recent memory (day 2); however, at the remote time point (day 12), memory retrieval was disrupted compared with the green light–off condition (Fig. 2F).

To further investigate the characteristics of PFC engram cells, we monitored transient calcium (Ca^{2+}) events in PFC cells in vivo. WT mice were injected with AAV_5-human synapsin1 (Syn): GCaMP6f in the PFC and implanted with a micro–gradient-index (GRIN) lens targeting the PFC (Fig. 2, G to I, and fig. S8) (*22*, *27*). On day 1, mice were first exposed to context B, followed by CFC in context A. Mice were then reexposed to both contexts in the same order on days 2 and 15 (Fig. 2J). The averaged frequency of Ca^{2+} events in PFC cells did not significantly change in either a time- or context-dependent manner (fig. S9B). However, a small but significant difference was revealed in the cumulative distribution curves of a rate difference index (assessing context selectivity; see the methods) between day 1 conditioning and day 15 recall and between day 2 recall and day 15 recall (fig. S9C). PFC cells did not appear to discriminate between the two contexts on day 1 before footshock presentation (Fig. 2, K and L). However, after footshock presentation, about 11% of cells showed a significant increase in Ca^{2+} transients [shock-responding (SR) cells] (Fig. 2, K and L). The remaining ~89% of PFC cells did not respond to the shocks [shock-nonresponding (SNR) cells]. The SR cells were less active than the SNR cells during exposure to contexts B and A on day 1 before footshock presentation (Fig. 2, L to N, and fig. S9D). During recall, the transient Ca^{2+} activity of SR cells in context A was significantly higher compared with that in context B on day 15, but not on days 1 or 2, whereas the frequency of Ca^{2+} transient events in SNR cells remained constant, irrespective of context (Fig. 2, M and N). This produced a significant rate difference index of Ca^{2+} activity for context A between the SR and SNR cells on day 15 but not on day 1 (excluding the shock delivery period) or day 2 (Fig. 2O). These results,

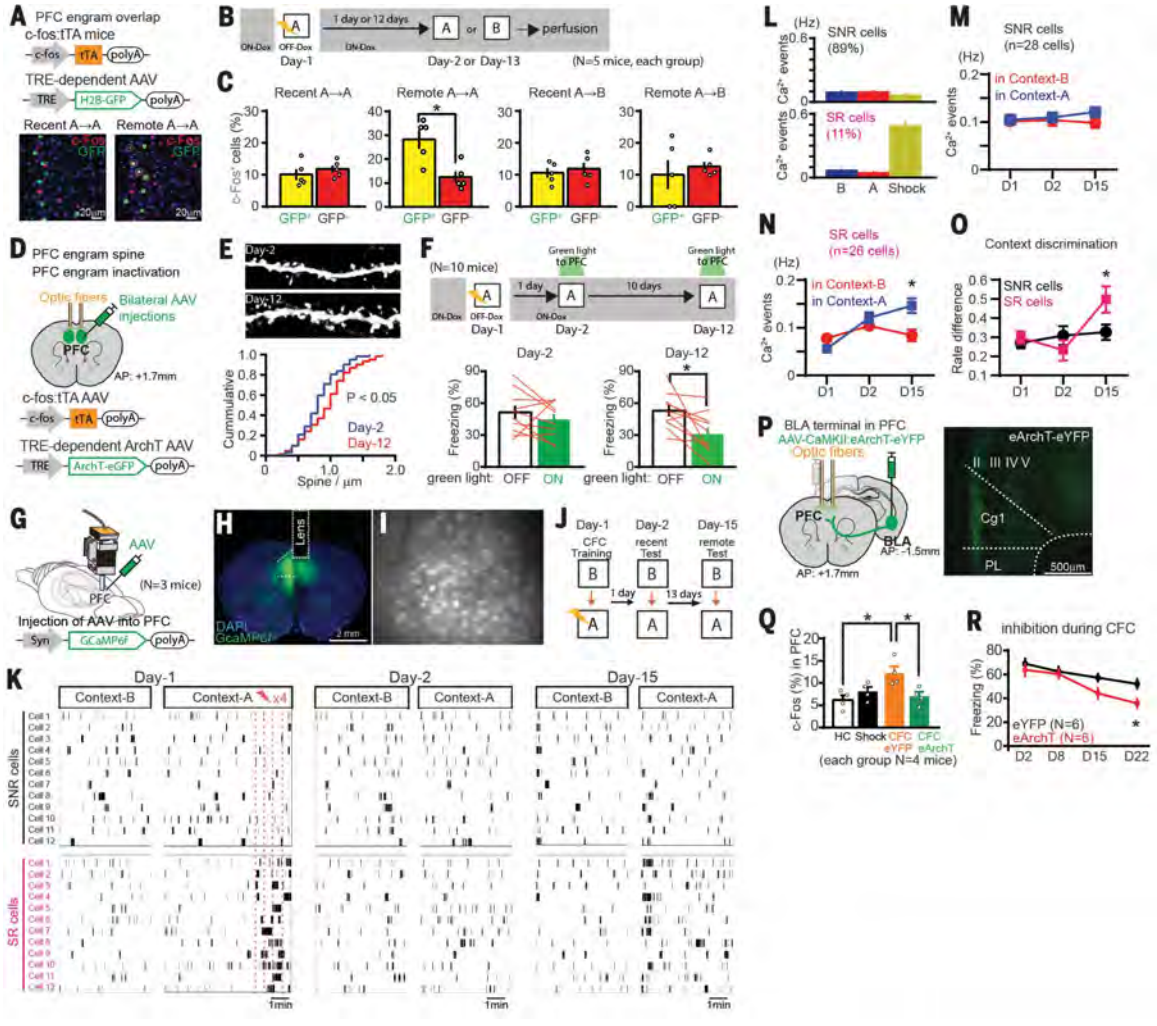

Fig. 2. PFC engram cells mature with time. (**A**) PFC engram cell labeling with H2B-GFP (top) and coronal sections of PFC with H2B-GFP (green) and anti–c-Fos (red) (bottom). Circled cells are double-positive. (**B**) Experimental schedule. (**C**) Percentages of c-Fos$^+$ cells in H2B-GFP$^+$ and H2B-GFP$^-$ cells in PFC. (**D**) PFC engram cell labeling with ArchT. (**E**) Dendritic spines from PFC engram cells (top) and cumulative probability of the spine density of PFC engrams (bottom). (**F**) Experimental schedule (top) and averaged freezing for green light–off and green light–on epochs during recall testing (bottom). (**G** and **H**) Viral injections and GRIN lens implantation. (**I**) Stacked image acquired through the microendoscope over 10 min of imaging in the PFC. (**J**) Experimental schedule. (**K**) Raster plots of Ca^{2+} events (black bars) in shock-nonresponding (SNR) and shock-responding (SR) cells in the PFC (showing 12 example cells). (**L** to **N**) Averaged Ca^{2+} event frequency for SNR and SR cells on days 1, 2, and day 15. (**O**) Averaged rate difference index of Ca^{2+} activity. (**P**) Viral injections and optic fiber implantations (left) and coronal sections of PFC visualizing BLA axons (green) (right). Cg1, cingulate cortex 1 (rACC). (**Q**) Percentages of c-Fos$^+$ cells in the PFC of the HC, shock only, CFC with eYFP, and CFC with eArchT groups. (**R**) Time courses of freezing during recall tests. *$P < 0.05$; unpaired t test [(C), (O), and (R)], Kolmogorov-Smirnov (KS) test (E), paired t test [(F), (M), and (N)], or one-way ANOVA with Tukey-Kramer test (Q). Graphs show means ± SEM.

combined with c-Fos activation data (Fig. 1, M to O), suggest that the SR cells may be the PFC memory engram cells, given that the generation of the PFC engram cells requires both context exposure and footshocks.

Our calcium imaging data suggest that footshock stimulus input into the PFC is crucial for the generation of PFC engram cells. Because the BLA integrates footshock information arriving from the thalamus (*28*) and projects to the PFC (figs. S5I and S10), we optogenetically inhibited the pathway from the BLA to the PFC during CFC (Fig. 2P). Optogenetic inhibition of BLA terminals in the PFC during CFC disrupted the generation of PFC engram cells (Fig. 2Q). The terminal inhibition during CFC also inhibited remote memory formation (Fig. 2R).

To test whether the HPC engram cells play a crucial role in the functional maturation of PFC engram cells during the systems consolidation process, we bilaterally targeted injection of AAV_9-TRE:tetanus toxin light chain (TeTX) or AAV_9-TRE:eYFP (as a control) to the hippocampal dentate gyrus (DG) of c-fos:tTA transgenic mice (Fig. 3A). When the mice were subjected to CFC, DG engram cells were labeled with TeTX. DG engram cell labeling with TeTX caused a robust inhibition of DG engram cell output, as revealed by greatly reduced immunoreactivity of vesicle-associated membrane protein 2 (VAMP2)—which is essential for activity-dependent neurotransmitter release from presynaptic terminals (*13*)—within the stratum lucidum in hippocampal CA3 in mice that were off doxycycline, compared with that in mice that were on doxycycline (Fig. 3, B and C). In TeTX-expressing mice, optogenetic activation of DG engram cells with ChR2 failed to produce the increase in CA3 c-Fos$^+$ cells that was observed in eYFP control mice relative to home-cage controls (Fig. 3D). TeTX expression in HPC engram cells inhibited the reactivation of PFC engram cells, compared with that in the eYFP control group, during exposure to context A 12 days after CFC (Fig. 3, E and F). TeTX expression also blocked the increase in the dendritic spine density of PFC engram cells that was observed in the eYFP group (Fig. 3G). In vivo calcium imaging revealed that TeTX expression in HPC engram cells after CFC blocked the increase in the context discrimination index in SR cells in the PFC (Fig. 3H and fig. S11).

To investigate the postconsolidation fate of HPC engram cells, we crossed c-fos:tTA transgenic mice with TRE:H2B–GFP transgenic mice (*29*), subjected them to CFC, then reexposed them to context A (the conditioned context) or context B (an unconditioned context) on day 2

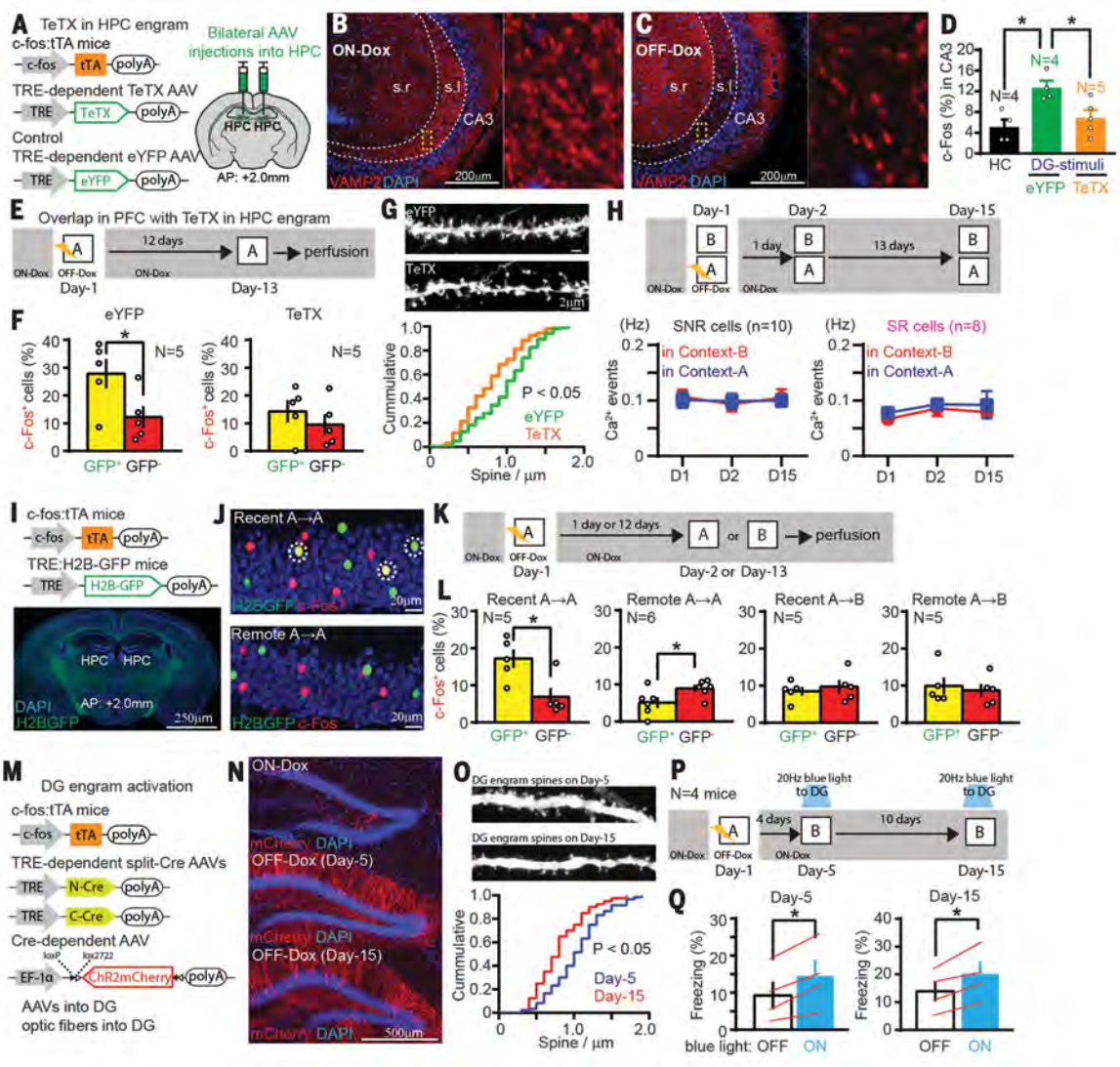

Fig. 3. HPC engram cells support the maturation of PFC engram cells and become silent with time. (**A**) DG engram cell labeling with TeTX. (**B** and **C**) Sagittal sections of HPC with anti-VAMP2 (red). The yellow box indicates the area of magnification (right). s.r., stratum radiatum; s.l., stratum lucidum. (**D**) Percentages of c-Fos$^+$ cells in hippocampal CA3 of the HC, blue light–on mice with eYFP, and blue light–on mice with TeTX. (**E**) Experimental schedule. (**F**) Percentages of c-Fos$^+$ cells in H2B-GFP$^+$ and H2B-GFP$^-$ cells in the PFC of eYFP- and TeTX-expressing mice. (**G**) Dendritic spines from PFC engrams (top) and cumulative probability of the spine density of PFC engrams in eYFP- and TeTX-expressing mice (bottom). (**H**) Experimental schedule (top) and averaged Ca^{2+} event frequency of SNR and SR cells under the TeTX-expressing condition (bottom). (**I**) Transgenic strategy of DG engram cell labeling with H2B-GFP (top) and coronal section of the brain (bottom). (**J**) Coronal sections of DG with H2B-GFP (green) and anti–c-Fos (red). Circled cells are double-positive. (**K** and **P**) Experimental schedules. (**L**) Percentages of c-Fos$^+$ cells in H2B-GFP$^+$ and H2B-GFP$^-$ cells in the DG. (**M**) Long-term DG engram cell labeling with ChR2. (**N**) Coronal sections of DG with ChR2-mCherry (red). (**O**) Dendritic spines from DG engrams (top) and cumulative probability of the spine density of DG engrams (bottom). (**Q**) Averaged freezing for blue light–off and blue light–on epochs. *P < 0.05; one-way ANOVA with Tukey-Kramer test (D), unpaired t test [(F) and (L)], KS test [(G) and (O)], or paired t test [(H) and (Q)]. Graphs show means ± SEM.

or 13 (Fig. 3, I to K). Compared with the non-engram cells, DG engram cells were preferentially reactivated in context A on day 2, but not on day 13 (Fig. 3L). No difference was observed in the activation of DG engram and non-engram cells by context B (Fig. 3L). We were unable to maintain labeled DG engram cells with ChR2 beyond 12 days with injection of AAV_9-TRE:ChR2-mCherry. To extend this technical limit, we targeted injections of $AAV_{1,5,8,9}$-TRE:CCre, $AAV_{1,5,8,9}$-TRE:NCre, and AAV_5-elongation factor 1a (EF1a):ChR2-mCherry to the DG of c-fos:tTA transgenic mice (Fig. 3M). We could thus extend viable labeling by a few days (Fig. 3N). The spine density of DG engram cells on day 15 was significantly reduced compared with that on day 5 (Fig. 3O and fig. S12). On both days 5 and 15, optogenetic activation of DG engram cells induced freezing behavior (Fig. 3, P and Q).

Last, we investigated the role of MEC-Va projections into the BLA in recent and remote memory (Fig. 4A and fig. S2A). Inhibition of MEC-Va terminals in the BLA during CFC disrupted contextual fear memory formation. Retrieval was impaired at all time points tested (Fig. 4B). When terminal inhibition was restricted to retrieval, recent memory tested on days 2 and 8 was impaired, but remote memory retrieval on days 15 and 22 was unaffected (Fig. 3C). In contrast, inhibition of PFC engram cell terminals in the BLA did not impair memory retrieval on day 2 but did impair memory retrieval on day 12 (Fig. 4, D and E). To investigate whether the BLA fear memory engram cells formed on day 1 are maintained and used for PFC engram-dependent remote memory recall, we subjected the double transgenic mice (Fig. 4, F and I) to CFC and reexposed them to context A at recent or remote time points (Fig. 4G). BLA engram cells were reactivated equally well by context A at recent and remote time points (Fig. 4H). Similarly, BLA cells activated by recent recall were reactivated equally well by reexposure to context A at recent and remote time points (Fig. 4, J and K).

In this study, we found that PFC memory engram cells for CFC were rapidly formed during day 1 training through inputs from both the MEC-Va and the BLA, but they were not retrievable with natural recall cues. The immature PFC engram cells functionally, structurally,

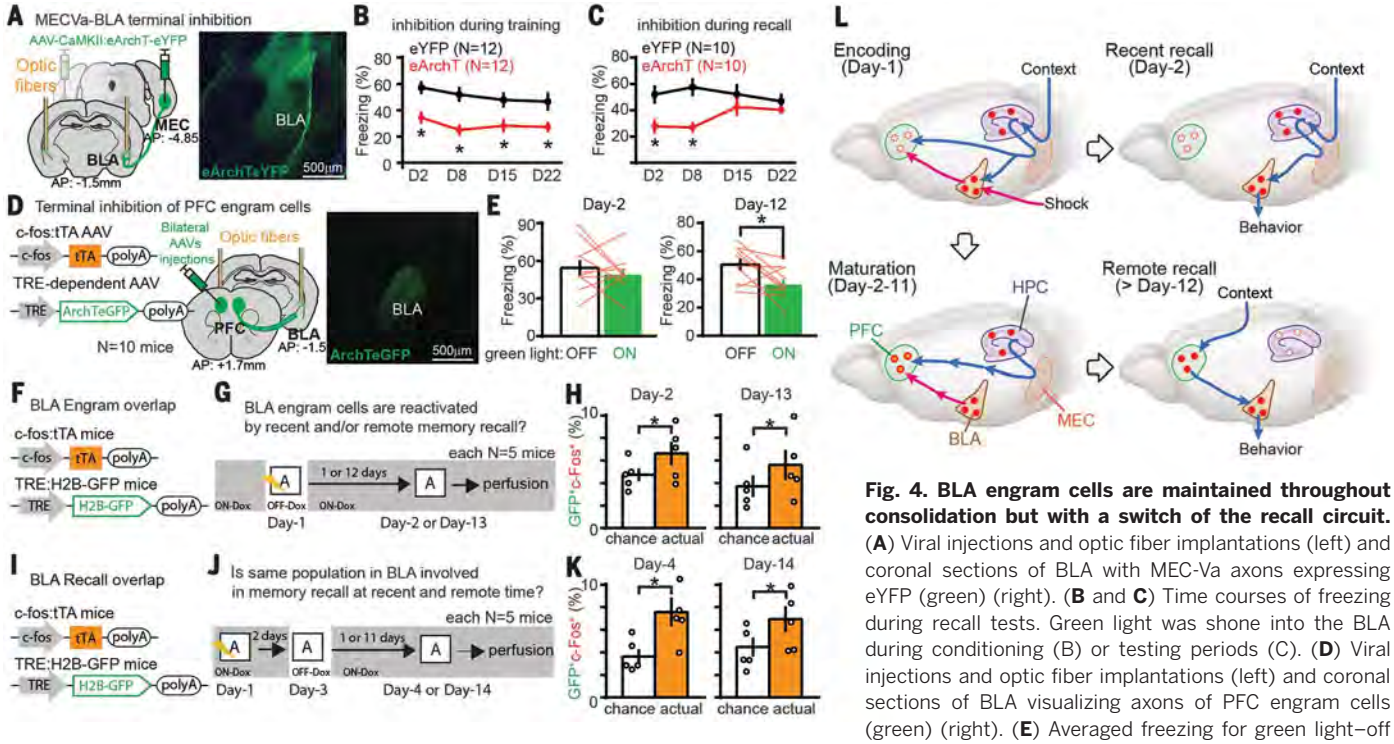

Fig. 4. BLA engram cells are maintained throughout consolidation but with a switch of the recall circuit. (**A**) Viral injections and optic fiber implantations (left) and coronal sections of BLA with MEC-Va axons expressing eYFP (green) (right). (**B** and **C**) Time courses of freezing during recall tests. Green light was shone into the BLA during conditioning (B) or testing periods (C). (**D**) Viral injections and optic fiber implantations (left) and coronal sections of BLA visualizing axons of PFC engram cells (green) (right). (**E**) Averaged freezing for green light–off and green light–on epochs during recall testing. (**F** and **I**) BLA engram cell labeling with H2B-GFP. (**G** and **J**) Experimental schedules. (**H** and **K**) Percentages of double-labeling with c-Fos and H2B-GFP in the BLA compared with the calculated chance percentages. (**L**) A new model for systems consolidation of memory. *$P < 0.05$; unpaired t test [(B), (C), (H), and (K)] or paired t test (E). Graphs show means ± SEM.

and physiologically matured during the subsequent few weeks, and this process required inputs from HPC engram cells, presumably through the MEC-Va. In contrast to their formation on day 1, retrieval of the PFC engram at a remote time did not require MEC-Va input. HPC engram cells that formed during training became silent with time; they were not retrieved on day 14 by natural recall cues but were still reactivatable optogenetically for recall. However, fear memory BLA engrams that formed during training were functionally maintained, even after the consolidation-mediated switch in recall circuits (Fig. 4L).

Our model (Fig. 4L) introduces the concept that the prefrontal memory engram is already generated, albeit in an immature form, on day 1 of training through inputs from both the HPC-EC network and the BLA (Fig. 1). The standard model (*1*, *2*, *4*, *6*, *7*, *11*) hypothesizes that remote memory is formed in the cortex by a slow transfer of hippocampal memory. In contrast, in our study, the role of the hippocampus in cortical memory is in the rapid generation of immature engram cells in the PFC during training and in the subsequent functional maturation of these preexisting engram cells (Fig. 2). The immature PFC engram may correspond to the cortical "tagging" suggested in an earlier study (*14*). In a previous study, the BLA was found to be crucial for both recent and remote fear memory expression (*30*). Our results demonstrate an overlapping set of BLA engram cells for both recent and remote fear memory retrieval, which were quickly formed during training (Fig. 4). However, the source of input into the BLA engrams for retrieval shifts from the MEC-Va at recent time points to the PFC engram at remote time points (Fig. 4L). The route through which contextual stimuli activate the mature PFC engram is unknown. Most likely, the information processed in a variety of sensory cortices reaches the PFC via the thalamus (*31*). Supporting this idea, PFC engram cells receive monosynaptic input from both the medial-dorsal and anteromedial thalamus (fig. S5).

Our finding of the lasting hippocampal engrams (Fig. 3Q) is consistent with multiple trace theory (*5*, *11*). However, at the postconsolidation stage, the hippocampal engrams were not activatable by natural recall cues, but rather by optogenetic stimulation. A similar state of hippocampal engrams has previously been observed in anisomycin-induced amnesia (*24*) and mouse models of early Alzheimer's disease (*26*), and the early (day 2) PFC engram cells showed a similar property (Figs. 1S and 2C). Although we did not determine how long after encoding this "silent state" of the hippocampal engram lasts, we speculate that the hippocampal engram eventually loses the original memory information (*29*, *32*, *33*). Alternatively, the silent engram cells may still participate in the successful remote recall of discrete episodic details (*5*, *11*).

As in previous studies (*18*, *20*, *29*), we observed that training resulted in widespread neuronal activation in the neocortex, including the ACC and RSC. However, whereas the activation of PFC neurons is crucial for formation of remote memory, MEC-Va input into the cACC or RSC is dispensable for this process. For remote memory, the PFC may thus have a distinctive role in integrating multiple sensory information stored in various cortical areas (*11*). Last, our data show that the remote memory expressed by the PFC engram is conditioned-context specific, suggesting that it is episodic-like.

REFERENCES AND NOTES

1. D. Marr, *Philos. Trans. R. Soc. London B Biol. Sci.* **262**, 23–81 (1971).
2. L. R. Squire, *Science* **232**, 1612–1619 (1986).
3. J. J. Kim, M. S. Fanselow, *Science* **256**, 675–677 (1992).
4. J. L. McClelland, B. L. McNaughton, R. C. O'Reilly, *Psychol. Rev.* **102**, 419–457 (1995).
5. L. Nadel, M. Moscovitch, *Curr. Opin. Neurobiol.* **7**, 217–227 (1997).
6. D. Tse *et al.*, *Science* **316**, 76–82 (2007).
7. J. L. McClelland, *J. Exp. Psychol. Gen.* **142**, 1190–1210 (2013).
8. G. Buzsáki, *Cereb. Cortex* **6**, 81–92 (1996).
9. A. G. Siapas, M. A. Wilson, *Neuron* **21**, 1123–1128 (1998).
10. B. J. Wiltgen, R. A. Brown, L. E. Talton, A. J. Silva, *Neuron* **44**, 101–108 (2004).
11. P. W. Frankland, B. Bontempi, *Nat. Rev. Neurosci.* **6**, 119–130 (2005).
12. A. R. Preston, H. Eichenbaum, *Curr. Biol.* **23**, R764–R773 (2013).
13. T. Nakashiba, D. L. Buhl, T. J. McHugh, S. Tonegawa, *Neuron* **62**, 781–787 (2009).
14. E. Lesburguères *et al.*, *Science* **331**, 924–928 (2011).
15. M. Zelikowsky, S. Bissiere, M. S. Fanselow, *J. Neurosci.* **32**, 3393–3397 (2012).
16. L. G. Reijmers, B. L. Perkins, N. Matsuo, M. Mayford, *Science* **317**, 1230–1233 (2007).
17. X. Liu *et al.*, *Nature* **484**, 381–385 (2012).

18. S. Tonegawa, X. Liu, S. Ramirez, R. Redondo, *Neuron* **87**, 918–931 (2015).
19. T. Kitamura *et al*., *Science* **343**, 896–901 (2014).
20. L. Ye *et al*., *Cell* **165**, 1776–1788 (2016).
21. K. Deisseroth, *Nat. Neurosci.* **18**, 1213–1225 (2015).
22. Y. Ziv *et al*., *Nat. Neurosci.* **16**, 264–266 (2013).
23. G. Sürmeli *et al*., *Neuron* **88**, 1040–1053 (2015).
24. T. J. Ryan, D. S. Roy, M. Pignatelli, A. Arons, S. Tonegawa, *Science* **348**, 1007–1013 (2015).
25. A. Hayashi-Takagi *et al*., *Nature* **525**, 333–338 (2015).
26. D. S. Roy *et al*., *Nature* **531**, 508–512 (2016).
27. T. Kitamura *et al*., *Neuron* **87**, 1317–1331 (2015).
28. B. A. Pellman, J. J. Kim, *Trends Neurosci.* **39**, 420–431 (2016).
29. K. K. Tayler, K. Z. Tanaka, L. G. Reijmers, B. J. Wiltgen, *Curr. Biol.* **23**, 99–106 (2013).
30. S. Maren, G. Aharonov, M. S. Fanselow, *Behav. Neurosci.* **110**, 718–726 (1996).
31. F. H. Do-Monte, K. Quiñones-Laracuente, G. J. Quirk, *Nature* **519**, 460–463 (2015).
32. C. A. Denny *et al*., *Neuron* **83**, 189–201 (2014).
33. T. Kitamura *et al*., *Cell* **139**, 814–827 (2009).

ACKNOWLEDGMENTS

We thank F. Bushard, J. Martin, T. Ryan, J. Yamamoto, C. Sun, W. Yu, S. Huang, M. Ragion, A. Arons, X. Zhou, C. Ragion, A. Moffa, L. Brenner, A. Hamalian, and D. King for help with experiments and preparing the manuscript; all members of the Tonegawa laboratory for their support; I. Wickersham for providing rabies virus; and Y. Shima and S. B. Nelson for providing TRE3G split Cre AAV. All data necessary to understand and assess the conclusions of this research are available in the supplementary materials. This work was supported by the RIKEN Brain Science Institute, the Howard Hughes Medical Institute, and the JPB Foundation (to S.T.). AAV_9–c-fos: tTA, AAV_9-TRE:ChR2mCherry, AAV_9-TRE:ArchTeGFP, AAV_9-TRE: TeTX, and AAV_9-TRE:eYFP were developed at the Massachusetts Institute of Technology by the group of S.T.; virus plasmids are available through a material transfer agreement.

SUPPLEMENTARY MATERIALS

www.sciencemag.org/content/356/6333/73/suppl/DC1
Materials and Methods
Supplementary Text
Figs. S1 to S12
References (*34*–*51*)

28 December 2016; accepted 14 March 2017
10.1126/science.aam6808